

# Synthesis and Characterization of Modified Bismaleimide/Polysulfone Semi-Interpenetrating Polymer Networks

Jamal Kurdi, Ashwani Kumar

National Research Council of Canada, Institute for Chemical Process and Environmental Technology, Montreal Road Campus, Ottawa, Ontario, K1A 0R6, Canada

Received 28 April 2005; accepted 11 December 2005

DOI 10.1002/app.23946

Published online in Wiley InterScience (www.interscience.wiley.com).

**ABSTRACT:** The present work reports a new method of preparing semi-interpenetrating polymer network (semi-IPN) membranes through *in situ* polymerization of bismaleimide (BMI) within polysulfone (PSF). It was found that BMI could be polymerized at ambient conditions in the presence of a proton donor and PSF without the use of an initiator or a catalyst. Chemical structure characterization of these semi-IPNs by Fourier transform infrared attenuated total reflection (FTIR-ATR) revealed the possibility of imide cleavage and formation of amic acid when BMI polymerization was continued for a longer time while X-ray photoelectron spectroscopy (XPS) revealed the protonation of imide nitrogen at shorter polymerization time. It was also found that size of

thermoset BMI phase within the PSF thermoplastic has a significant impact on glass-transition temperature of resulting semi-IPN. By controlling the thermoset/thermoplastic phase separation of semi-IPNs through dope composition and formation techniques, gas separation membranes with comparable selectivity and permeance that were up to 12 times higher than corresponding PSF membranes were formed. © 2006 Wiley Periodicals, Inc. *J Appl Polym Sci* 102: 369–379, 2006

**Key words:** semi-interpenetrating networks (semi-IPN); gas permeation; FTIR; X-ray photoelectron spectroscopy (XPS); membranes; high performance polymers (BMI, PSF)

## INTRODUCTION

Polymeric membranes have been commercially recognized in many industrial applications as a rapidly growing green technology.<sup>1</sup> However, membranes produced from commercial polymeric materials suffer from a trade off between permeability and selectivity that reduces membrane performance and its commercialization in some applications such as separation of oxygen from air.<sup>2</sup> Baker emphasized the need for material development as one of the major strategies to improve membrane performance.<sup>3</sup> It is known that polymer blending can be used to modify membrane properties or/and to reduce the price of these materials as reported elsewhere.<sup>4</sup> The advantage of using polymer-based composites is the ability to create large variety of materials with tailor-made properties that could be suitable for membrane formation. Polymer blends that particularly structured at submicrometer scale are usually used to obtain unique combination of properties, which are impossible to achieve with classical blends or by only one polymer as illustrated elsewhere.<sup>5</sup> In this field, formation of interpenetrating

polymer networks (IPNs) was recognized for long time as a very useful means to create distinct multipolymer combinations.<sup>6</sup> *In situ* polymerization or crosslinking of one or more of monomers or oligomers inside and through another network usually leads to formation of interpenetrating fine multidomains having sizes of tens of nanometers as illustrated and reported elsewhere.<sup>7</sup> It was also emphasized that tailoring the interfaces of IPNs is necessary to obtain desired properties and overcome challenges such as defects in the fine structure,<sup>8</sup> phase separation,<sup>9</sup> and incompatibility.<sup>10</sup>

The importance of IPNs formation process to tailor gas or liquid transport characteristics which were correlated with the chemical structure and matrix morphology was recognized by several groups.<sup>11–14</sup> For example, the influence of synthesis conditions and compositions of polyurethane–polystyrene IPNs on their gas transport characteristics was illustrated.<sup>11</sup> These characteristics were influenced by the homogeneity and crosslinked nature of IPNs that should be controlled to prepare membranes suitable for gas separations.<sup>12–13</sup> On the other hand, the formation of defect-free ultrathin skinned asymmetric membranes should also be optimized to maximize membrane productivity as summarized elsewhere.<sup>4</sup> Therefore, the concept of synthesis of IPNs seems to be useful for development of multiphase polymeric membrane materials for gas separation processes as there is a distinct

NRCC No. 47867.

Correspondence to: A. Kumar (ashwani.kumar@nrc-cnrc.gc.ca).

possibility to control composite material properties and morphology. In the IPN class materials, semi-IPNs formation led to an improvement in the stability of phase morphology and mechanical properties of multiphase polymer systems<sup>15</sup> whereas the selected chemistry of IPN polymerization (i.e., crosslink density and grafting) led to a wide variety of morphologies.<sup>16</sup> It was also reported that the kinetics of the morphology development during processing plays an important role in controlling the final structure and properties of the matrix-based composite systems.<sup>17</sup> Therefore, it is necessary to select the appropriate chemistry and processing for the formation of semi-IPNs that could be suitable for a specified application such as gas separation membranes.

Bismaleimide (BMI) was used successfully in many high-performance thermoplastic polymers for formation of semi-IPNs. For example, BMI/polysulfone semi-IPN was prepared from a casting solution of BMI, polysulfone (PSF), and anionic initiator (1,4-diazabicyclo-[2,2,2]-octane) in *N*-methylpyrrolidone (NMP) solvent. Thermal polymerization of BMI was achieved in the cast film. However, optical microscopy of these films at a magnification of  $\times 1200$  showed phase separation.<sup>18</sup> It appears that the presence of a stagnant film at elevated temperature (120–270°C) enhanced the phase separation particularly before film drying and BMI polymerization. Liou et al.<sup>19</sup> reported an improvement in the synthesis of semi-IPN when BMI oligomer/polyimide was mixed in a rotary roller for 24 h within a highly viscous NMP/polyimide solution. They considered that BMI oligomers might act as a plasticizer for polyimides and led to formation of semi-IPNs containing microphase domains that are smaller than 0.25  $\mu\text{m}$ , which is beyond the resolution limit of optical polarized microscopy. Phenomenon of phase separation of thermoset/thermoplastic systems was illustrated by Bonnet et al.<sup>20</sup> The ability to prevent phase separation by interlocking the constituents of the networks (i.e., formation of the IPNs) before phase separation in addition to terminating polymerization process at a stage on or near the gel point was disclosed in a US patent.<sup>21</sup> It was clear from the above literature that processing and formation sequence play an important role in determining the morphology and properties of the final cured networks. In this work, we proposed a new procedure to prepare BMI/PSF semi-IPN membranes, which is different from literature<sup>18,22</sup> particularly in avoiding phase separation and gel formation before the coagulation step.

## EXPERIMENTAL

### Materials

Aromatic polysulfone (PSF; Udel® P-1700 NT LCD) was supplied by Solvay Advanced Polymers, USA in

**TABLE I**  
Compositions of Polymeric Solutions Used  
in This Study

Samples	Composition (% w/w)				
	PSF	NMP	BMI	EtOH	i-PrOH
PSF-EtOH	19.5	67.2	0	13.3	0
PSF-i-PrOH	19.5	67.2	0	0	13.3
PSF-BMI-EtOH	17.6	67.2	1.9	13.3	0

pellet form and was dried in an oven at 150°C for 8 h. Anhydrous 1-methyl-2-pyrrolidinone (Aldrich, 99.5%, reagent grade, water < 0.005%), 1,1'-(methylenedi-4,1-phenylene) bismaleimide 95% and anhydrous isopropanol 99.5% were supplied by Sigma-Aldrich, Canada. Anhydrous ethyl alcohol (EtOH) was received from Commercial Alcohols, ON, Canada. Hexanes of ACS reagent grade were supplied by VWR, Canada. All solvents were used as supplied under a dry nitrogen atmosphere. Ultra high purity Helium and medical air were supplied by BOC Gases, Canada and used as received without further purification.

### Membrane preparation

Samples of PSF with and without 1,1'-(methylenedi-4,1-phenylene) bismaleimide (BMI) were prepared as flat asymmetric membranes by sol-gel technique. Polymerization of BMI monomer was carried out in polymeric solutions containing anhydrous 1-methyl-2-pyrrolidinone (NMP) as an aprotic dipolar solvent and anhydrous EtOH. PSF (Udel P-1700 NT LCD) was selected due to its ability to form high-strength membrane and give favorable pore size distribution. Additionally, presence of low level of cyclic dimer that might precipitate in the polymeric solutions was also desirable. Ethanol (EtOH) was selected because it acts as a diluent<sup>23</sup> for forming the porous structure and as a proton donor to enhance anionic polymerization of BMI. The ratio (w/w) of BMI to PSF was selected to be less than 11% as a higher concentration might lead to the formation of a brittle polymer network. The weight percent composition of the nonsolvent in the dope was kept at one-fifth of NMP so that the final solution was close to its clouding point.<sup>24</sup> On the basis of these criteria, three different polymer solutions with varying compositions (Table I) were prepared by mixing PSF with or without BMI in NMP. After PSF was completely dissolved, the nonsolvent was mixed in this solution until a clear homogenous solution was obtained, and then BMI was dissolved in the solution. Mixing of these solutions was continued under normal light for 30–100 days.

Membrane films were prepared by casting homogenous solutions at room temperature on a clean glass plate placed in glove box equipped with a gas filter.

After casting each sample with a doctor knife having a gap of 250  $\mu\text{m}$ , the plate was quickly immersed in ambient-temperature distilled water. The membrane films were left in water for 3 days and then washed and stored in an anhydrous EtOH bath for 1 day. Membranes were subsequently placed in hexanes for 1 day before leaving them in a fume hood for 1 day. Drying was carried out at 80°C in air-purging convection oven for 1 day and finally in vacuum oven at 80°C and 725 mm Hg pressure for 2 days. Three circular coupons of 7.4 cm diameter were cut from each sample to be used in the permeation test while other pieces were cut from the same membrane for characterization. Membranes used in the permeation test were coated with silicon rubber. A solution of 3% Sylgard 184 (with a catalyst to base rubber ratio of 1:10) in *n*-pentane was sprayed as a thin layer on the top surface of the membrane and the solvent was allowed to evaporate. Application of four coatings was found to be adequate for making a gas separation membrane. Finally, the coated silicon rubber was cured in air-purging convection oven at 80°C for 1 day.

### Microscopy studies

Surface of each membrane before silicon rubber coating was examined using a Leica DMRXE optical microscope (Leica Microsystems Wetzlar GmbH, Wetzlar, Germany) equipped with bright/dark field illumination. Microscope was set at reflected light mode using the reflected light bright/dark field objectives (Delta optics PL Fluotar series) at standard magnifications of 50, 100, 200, 500, and 1000. Images were adjusted to be on a part of the surface that showed a thermoset/thermoplastic phase separation and an image was captured at magnification of 1000 times with Orthomat® E camera mounted on the microscope using Polaroid 72 black and white instant sheet films (ISO 400). An image of the microscope scale (graticule) was captured under identical conditions to scale the produced image.

Fourier transform infrared attenuated total reflection (FTIR-ATR) analysis was performed using a SuperCharged ZnSe single-bounce ATR crystal with a tensor FTIR spectrometer (Bruker IFS 66). The spectra were taken with 200 scans at a resolution of 4  $\text{cm}^{-1}$  in the range of 400–4000  $\text{cm}^{-1}$ . The FTIR-ATR background was performed at the same conditions without a sample in place. For X-ray photoelectron spectroscopy (XPS) experiments, each sample was mounted on a piece of conductive carbon tape. The samples were analyzed as received, using the Kratos AXIS Ultra XPS equipped with a hemispherical analyzer, a DLD (delay line detector), charge neutralizer, and a monochromatic Al  $K\alpha$  X-ray source. Analyses were performed using an accelerating voltage of 14 kV and a current of

10 mA. Survey scans were performed at a pass-energy of 160 eV. Species detected by survey scan were then analyzed at a pass-energy of 40 eV and quantified. The FTIR-ATR and XPS tests were carried out on membrane samples without silicon rubber coating.

### Thermal analysis

A TA instrument model 2920 Modulated differential scanning calorimetry, DSC V2.6 A, calibrated with Indium at 156.5985°C and with Tin at 231.93°C was used to measure the glass-transition temperature ( $T_g$ ). Under a nitrogen atmosphere, polymer samples were ramped to 50°C at 1°C/min, held isothermally for 10 min, and then heated to 350°C at 10°C/min. The  $T_g$  was calculated at the point of inflection of the DSC curve.

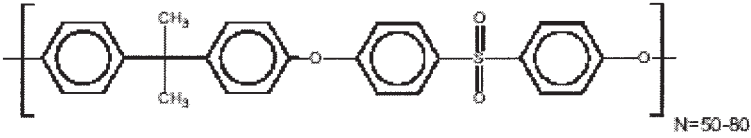
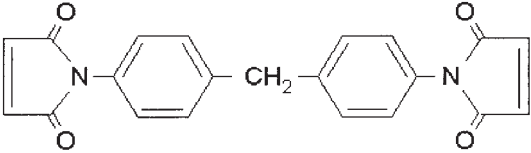
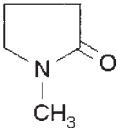
### Permeation test

A cross-flow test cell having a permeation surface area of 9.6  $\text{cm}^2$  was used. Medical air was used at feed pressure of 665 kPa gauge (498.8 cm Hg) and the retentate was set at a flow rate of 400 mL (STP)/min. Permeate was discharged to atmosphere. The permeate flow rate was measured by a soap bubble flow meter and the oxygen concentration in permeate was determined by gas chromatography. The measurement was taken as an average value for three different membranes made from the same solution at identical conditions.

## RESULTS AND DISCUSSION

Preliminary experiments were conducted in our lab to set appropriate experimental procedures. We have observed that BMI could be polymerized slowly inside PSF/NMP solutions in the presence of a proton donor. This polymerization process does not need initiators or additional catalysts, and have the advantage of using green chemical components such as EtOH, *i*-PrOH, BMI, and PSF. Also NMP is not on the hazardous air pollutants (HAPs) list of the 1990 Clean Air Act Amendments and it is both recyclable by distillation and readily biodegradable (Lyondell Chemical Company, USA). All experiments were done at ambient conditions. The chemical structure of PSF, BMI, and NMP are shown in Table II. Polymerization of BMI was indicated by color change and viscosity increase of polymeric solutions. In the case of EtOH as a proton donor, the color of the polymeric solution underwent gradual change from light yellow to a bright reddish-purple color after a long period of time accompanied with an increase in the viscosity of the solution. The red color indicates an anionic polymerization of BMI, which leads to a low-molecular-weight polymer compared to that from a radical polymerization as dis-

TABLE II  
Chemical Structure of PSF, BMI, and NMP

Component	Chemical structure
PSF (UDEL)	
BMI	
NMP	

cussed elsewhere.<sup>25</sup> On the basis of pulse radiolysis and electron spin resonance studies,<sup>26,27</sup> this BMI polymerization might be also described as shown in Scheme 1. The time required for these changes and the rate of polymerization depend on the concentration of ingredients, viscosity, mixing rate, and conditions such as pressure, temperature, and energy ray. At ambient lab conditions, it took up to 40 days to notice the change in the color and up to 80 days to reach its brightest color; then the solution started to appear cloudy, and the color changed to brownish red. Phase separation was clearly observed through precipitation of one of the polymeric phases. The last phenomenon is well known in literature<sup>15,18</sup> for the phase separation of thermoset/thermoplastic polymeric blends particularly for BMI/PSF blends. We also found that membranes formed with unclear or cloudy polymeric solution showed poor performance. Similar observations were made when *i*-PrOH instead of EtOH was used as a proton donor. However, the change in the color was from light yellow to a bright yellow. This might be due to different polymerization mechanism as it was reported that purple or red color indicates the anionic polymerization of BMI.<sup>25</sup> Absence of purple color in the case of *i*-PrOH might indicate that BMI probably underwent a free radical polymerization as shown in Scheme 2 and reported elsewhere.<sup>28</sup> However, anionic

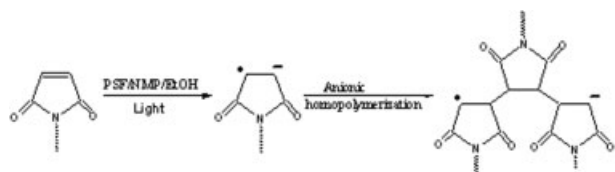
polymerization of BMI using EtOH was reported in this work whereas complete study with *i*-PrOH would be reported later. We also found that increasing the temperature to 50°C or irradiating with ultraviolet light accelerated BMI polymerization. However, slow polymerization accompanied with mixing allows slow growth of the thermoset phase size and the ability to control phase separation during the formation of semi-IPNs. Terminating polymerization of BMI prior to phase separation could be accomplished by solidifying the composite through coagulation and membrane formation by phase inversion process.

It was interesting to note that attempts to polymerize BMI under the same conditions as discussed above but in the absence of PSF did not succeed even after mixing for 100 days. This clearly indicated that PSF had an important role, perhaps as a catalyst, in BMI polymerization. The catalysis role of PSF could be similar to that found by nanocrystalline titania.<sup>29</sup> Furthermore, polymerization of BMI under same conditions did not occur in the absence of EtOH, indicating the vital role of a proton donor in this process.

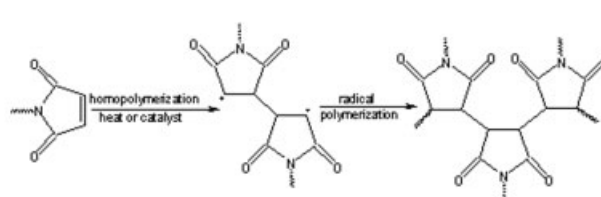
### Chemical structure analysis

#### FTIR-ATR analysis

FTIR-ATR spectra for PSF-EtOH, PSF-*i*-PrOH, PSF-BMI-EtOH-S, and PSF-BMI-EtOH-L membranes in the



Scheme 1 Anionic polymerization of BMI (∞ represents the rest of BMI molecule).



Scheme 2 Radical homopolymerization reaction of BMI.

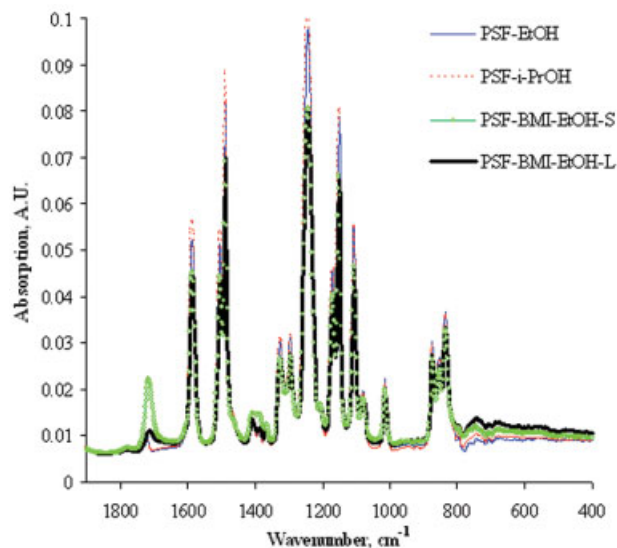


**Figure 1** FTIR-ATR spectra of polysulfone-based membranes. [Color figure can be viewed in the online issue, which is available at [www.interscience.wiley.com](http://www.interscience.wiley.com).]

range of 400–1900  $\text{cm}^{-1}$  were shown in Figure 1. The additional S and L symbols refer to solutions that were mixed for 40 and 80 days, respectively. As there were no bands in the range of 1800–1900  $\text{cm}^{-1}$ , this was set as a baseline for all spectra. Spectra were also normalized in a way that each spectrum has the same area under the curve within the range of 400–1900  $\text{cm}^{-1}$ .<sup>30</sup> It is also possible to normalize these spectra to a suitable reference band. The reference band could be at 854  $\text{cm}^{-1}$ , which is assigned to 1,4 aromatic (*para*-disubstitued phenyl ring)<sup>31</sup> found in both PSF and BMI and does not influence by contributions. It was observed that both of these methods gave results with slight differences. We have normalized the bands on the basis of area over 400–1900  $\text{cm}^{-1}$  in sense that the area of each band became relative to the sum of areas of all bands in the spectrum excluding the functional part. As shown in Figure 1, aromatic bands could be located at 834  $\text{cm}^{-1}$  assigned to out-of-plane CH bending in *para*-substitued aromatics,<sup>32</sup> at 1013 and 1106  $\text{cm}^{-1}$  assigned to in-plane CH bending in the *p*-phenylene groups,<sup>33</sup> and at 1488, 1503, and 1585  $\text{cm}^{-1}$ , which are characteristics of benzene rings.<sup>34,35</sup> The intensity of these bands decreased in the spectra of membranes containing BMI because the incorporated BMI contains less benzene rings than PSF. Additional contribution by other functional groups might also exist. The band at 834  $\text{cm}^{-1}$  might be associated with the carbonyl bending in imide group found in BMI.<sup>36</sup> The band at 1013  $\text{cm}^{-1}$  might be also assigned to asymmetric C—C—O stretching in primary alcohols<sup>37</sup> and at 1106  $\text{cm}^{-1}$  to asymmetric C—O stretching in adsorbed alcohols.<sup>38</sup>

Band at 1243  $\text{cm}^{-1}$  was assigned to Ar—O—Ar asymmetrical stretching.<sup>39–41</sup> The decrease in this

band for membranes containing BMI was due to the absence of ether group in BMI. Band at 1080  $\text{cm}^{-1}$  was assigned to Ar—O—Ar symmetrical stretching.<sup>41</sup> Bands at 1364 and 1387  $\text{cm}^{-1}$  are associated with methyl group and they might be assigned to  $\text{CH}_3$  symmetrical bending umbrella mode of gemdimethyl group in PSF<sup>37,42</sup> or  $\text{CH}$  bending of  $\text{CH}_2$  in BMI.<sup>43</sup> Incorporation of BMI, which contains less methyl groups than PSF might lead to a decrease in the intensity of these two bands. However, there are other contributions from the symmetric and asymmetric C—N—C stretching that might be attributed to imide of BMI<sup>31</sup> with opposite influences. The bands associated with sulfone groups were determined by their maxima located at 1151 and 1324  $\text{cm}^{-1}$ , and assigned to symmetric and asymmetric sulfone stretching respectively.<sup>41</sup> Their intensity decrease for membranes containing BMI was clearly shown in Figure 1 and was attributed to the absence of sulfone group in the incorporated BMI.

It was worth noting that three ranges in the spectra located at 715–800, 1350–1430, and 1660–1740  $\text{cm}^{-1}$  had undergone significant changes and should be closely analyzed. In the first range as shown in Figure 2, bands around 745, 760, and 795  $\text{cm}^{-1}$  were assigned to aromatic CH out-of-plane bending.<sup>44</sup> Other contributions from different groups might also be involved. Two bands at 745 and 760  $\text{cm}^{-1}$  might be associated with C—N symmetrical stretching in the imide groups.<sup>45</sup> Therefore, the increase in the intensity of these bands could be observed upon incorporation of BMI as it contains imide groups (Fig. 2). The bands at 760 and 795  $\text{cm}^{-1}$  might also be assigned to O—H

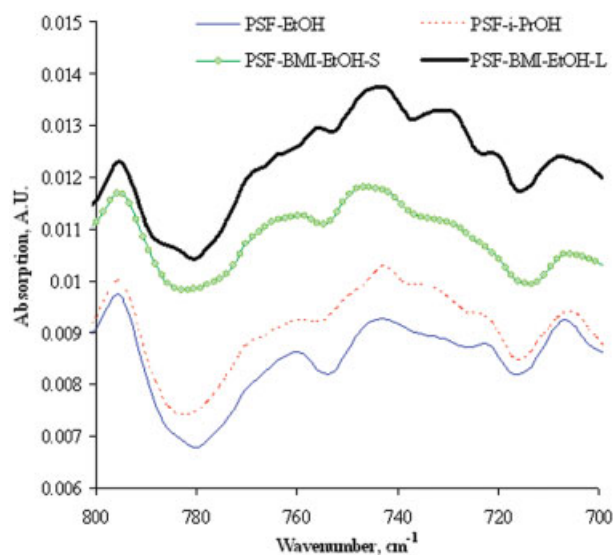


**Figure 2** FTIR-ATR spectra of polysulfone-based membranes that show the aromatic CH out-of-plane bending bands. [Color figure can be viewed in the online issue, which is available at [www.interscience.wiley.com](http://www.interscience.wiley.com).]

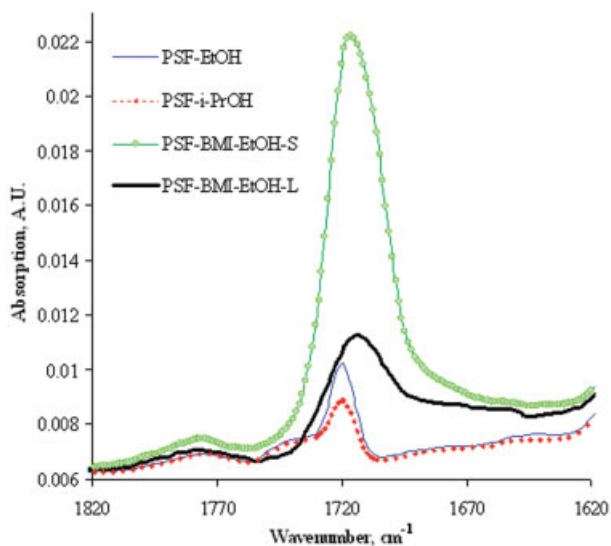


**Figure 3** FTIR-ATR spectra of polysulfone-based membranes in the carbonyl group range. [Color figure can be viewed in the online issue, which is available at [www.interscience.wiley.com](http://www.interscience.wiley.com).]

deformation<sup>46</sup> or out-of-plane N—H bending.<sup>47</sup> This might indicate the presence of a trace amount of OH or NH groups in PSF-BMI-EtOH-L membranes compared to all other membranes. In the second range, the bands at 1364 and 1387  $\text{cm}^{-1}$  were primarily assigned to  $\text{CH}_3$  symmetrical bending as discussed above whereas the band at 1409  $\text{cm}^{-1}$  was assigned to CH bending and aromatic ring modes.<sup>37</sup> However, additional significant contribution found for the band at 1387  $\text{cm}^{-1}$  in the spectra of PSF-BMI-EtOH-S could be attributed to imide group in the incorporated BMI.<sup>48</sup> The decrease in the intensity of this band for the spectrum of PSF-BMI-EtOH-L could be due to a possible cleavage of some imide groups by a trace amount of water.

The spectra of the third range were plotted in Figure 3 to clearly analyze the results. Both PSF-EtOH and PSF-i-PrOH membranes showed a small amount of cyclic imide at 1719 and 1775  $\text{cm}^{-1}$  that might be attributed to contamination by BMI occurred within the baths used after membrane coagulation. The presence of residual NMP in these membranes might be another possibility but the carbonyl of pure NMP usually has its band around 1695  $\text{cm}^{-1}$  or around 1670  $\text{cm}^{-1}$  for a complexed NMP.<sup>49</sup> The strongest intensity of the cyclic imide bands was found for spectrum of PSF-BMI-EtOH-S due to the incorporated BMI that contains cyclic imide. However, there was a decrease in the intensity of these two bands for PSF-BMI-EtOH-L. This might be attributed to cleavage of the cyclic imide group and possible formation of amic acid.

The FTIR-ATR functional group region between 2000 and 4000  $\text{cm}^{-1}$  was shown in Figure 4. The

significant differences among spectra were located between 3090 and 4000  $\text{cm}^{-1}$ . The overtone carbonyl imide stretch is usually located within a broad band centered at 3485  $\text{cm}^{-1}$ . However, this band might shift to a lower wavenumber upon association as illustrated elsewhere.<sup>50</sup> Therefore, the increase in the spectrum intensity of PSF-BMI-EtOH-S might be attributed to associated imide that came from the incorporated BMI. This intensity was found to increase for PSF-BMI-EtOH-L that might be attributed to additional incorporation of complexed NMP and/or EtOH to amic acid<sup>51,52</sup> resulted from imide cleavage. This could be supported by the fact that the absorption bands characteristic of aromatic amic acids are in the range of 2900–3200  $\text{cm}^{-1}$  as reported elsewhere.<sup>53</sup> The broad bands between 3200 and 3600  $\text{cm}^{-1}$  might be attributed to the hydrogen bonded NH and OH groups.<sup>54,55</sup> The characteristic amide band is located within the 3240–3320  $\text{cm}^{-1}$  range as reported elsewhere.<sup>56</sup> The band at 3260  $\text{cm}^{-1}$  might be assigned to NH stretching that involves hydrogen bonding.<sup>57,58</sup> The band at 3258  $\text{cm}^{-1}$  might be assigned to —OH of the —COOH groups and other —OH groups.<sup>40</sup> The band around 3400  $\text{cm}^{-1}$  was assigned to OH stretching of coordinated water or alcohol.<sup>58</sup> This might indicate that amic acid caused to incorporate a small amount of complexed NMP as might be described by Scheme 3 and possible alcohol or water was the reason for increase in the band intensity of PSF-BMI-EtOH-L compared to PSF-BMI-EtOH-S within the 3090–4000  $\text{cm}^{-1}$  range.

#### XPS analysis

The XPS provides useful information about chemical composition of the surface of membrane materials.

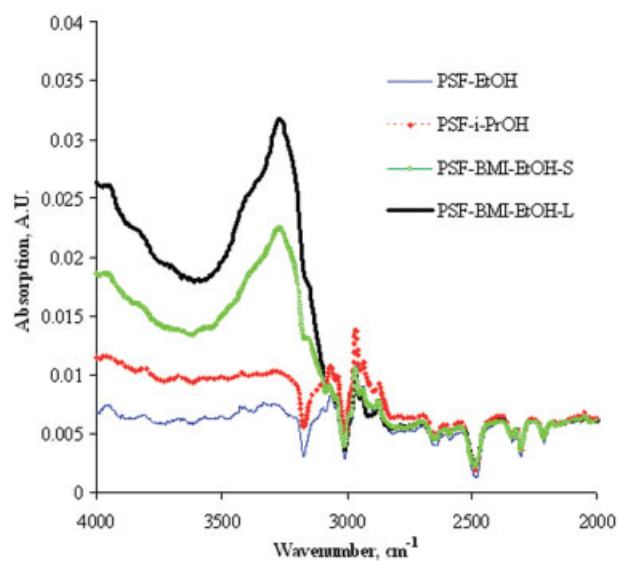


**Figure 4** FTIR-ATR functional group region spectra of polysulfone-based membranes. [Color figure can be viewed in the online issue, which is available at [www.interscience.wiley.com](http://www.interscience.wiley.com).]



**Scheme 3** Imide cleavage that leads to formation of amic acid and then complexation with NMP.

The XPS core-level spectra for PSF-EtOH, PSF-*i*-PrOH, PSF-BMI-EtOH-S, and PSF-BMI-EtOH-L membranes were shown in Figures 5–8 for elemental carbon, oxygen, nitrogen, and sulfur respectively. The strongest band in each spectrum was assigned to carbon bonded with another carbon or hydrogen atom, as this type of carbon atom has the highest atomic concentration in all possible combination of used components as shown in Table III. The maximum of this band was corrected to be 285 eV as illustrated elsewhere.<sup>59</sup> This charge correction was applied to the whole spectrum in each sample. For the purpose of comparison, the base line where there is no band was adjusted to be at the same level for all spectra in each figure. As shown in Figure 5, four bands could be observed that might be assigned to carbon bonded to another carbon or/and hydrogen including aromatics centered at 285 eV,<sup>59</sup> carbon has a single bond with nitrogen or oxygen located between 286 and 287 eV<sup>60,61</sup> as in ether or alcohol, carbonyl carbon in imide group located between 288.5 eV and 288.8 eV,<sup>59,62</sup> and shake up satellite of phenyl groups from  $\pi$  to  $\pi^*$  located between 290 and 294 eV.<sup>32,63</sup> The decrease in the first band at 285 eV upon BMI incorporation was attributed to lower

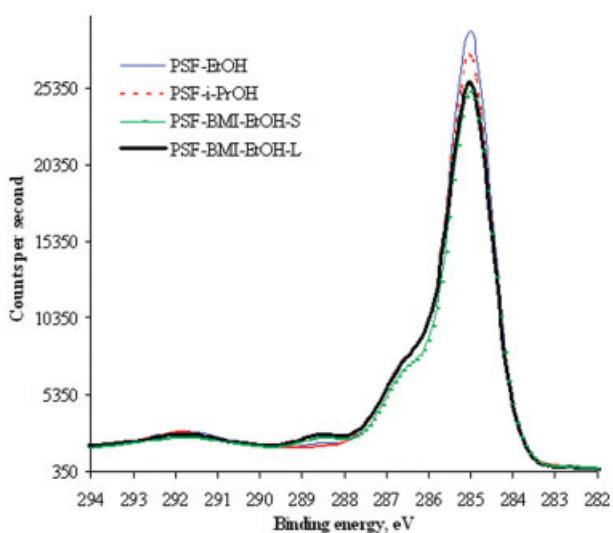


**Figure 5** High-resolution XPS core-level spectra of elemental carbon for polysulfone-based membranes. [Color figure can be viewed in the online issue, which is available at [www.interscience.wiley.com](http://www.interscience.wiley.com).]

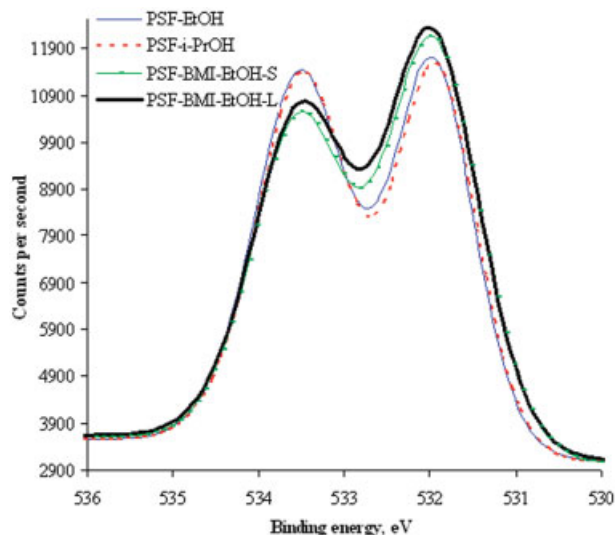


**Figure 6** High-resolution XPS core-level spectra of elemental oxygen for polysulfone-based membranes. [Color figure can be viewed in the online issue, which is available at [www.interscience.wiley.com](http://www.interscience.wiley.com).]

concentration of this carbon type in BMI than in PSF as shown in Table III. The small differences between spectra of PSF-EtOH and PSF-*i*-PrOH as well as between PSF-BMI-EtOH-S and PSF-BMI-EtOH-L membranes could be attributed to experimental error or to presence of trace residual solvents. The second band overlaps with the first band that makes it not suitable to obtain useful information. The third band centered at 288.7 was the strongest for spectra of PSF-BMI-EtOH-L than all other membranes due to presence of BMI and possible NMP residual. Both BMI and NMP

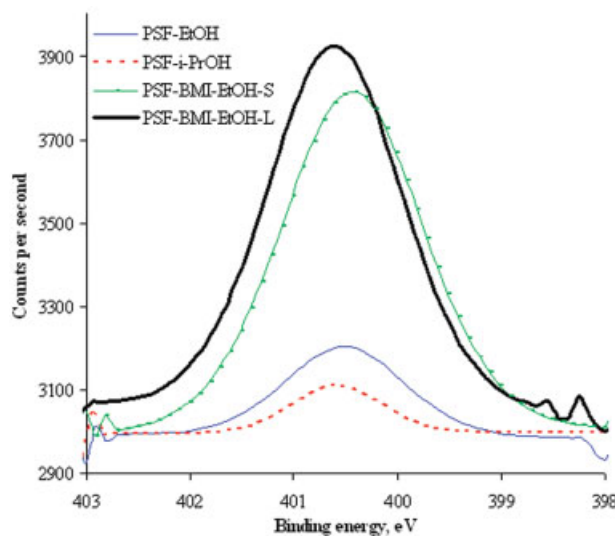


**Figure 7** High-resolution XPS core-level spectra of elemental nitrogen for polysulfone-based membranes. [Color figure can be viewed in the online issue, which is available at [www.interscience.wiley.com](http://www.interscience.wiley.com).]

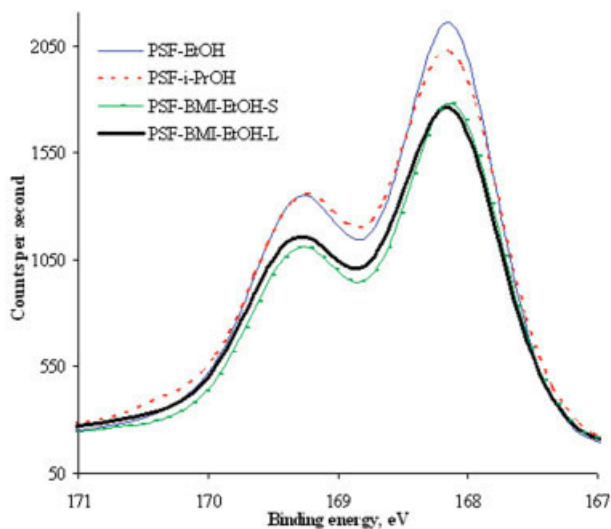


**Figure 8** High-resolution XPS core-level spectra of elemental sulfur for polysulfone-based membranes. [Color figure can be viewed in the online issue, which is available at [www.interscience.wiley.com](http://www.interscience.wiley.com).]

contain carbonyl carbons that are absent in other components as seen in Table III. The final shake up band showed slight differences among all spectra with a decrease in the intensity for spectra of membranes containing BMI, as this component has a lower aromatic concentration than PSF.

The core-level spectra of elemental oxygen were shown in Figure 6. The two main bands were assigned to carbonyl oxygen centered at 532 eV and ether oxygen centered at 533.5 eV.<sup>32,60</sup> It was clear that upon BMI incorporation, the carbonyl oxygen band increased and the ether oxygen decreased. This might be attributed to the presence of carbonyl oxygen in BMI but the presence of ether oxygen in PSF as shown in Table III.

The core-level spectra of elemental nitrogen were shown in Figure 7. It was surprising that PSF membranes prepared from NMP/alcohol solutions showed a small band for elemental nitrogen in their XPS spectra. This amount was slightly higher when EtOH was used instead of *i*-PrOH in the casting solution. The

same result was revealed early by FTIR-ATR indicating the validity of presence of nitrogen within PSF membranes. Because PSF membranes without BMI were soaked in the same baths with the membranes containing BMI, it might be because slight amount of BMI containing nitrogen was transferred to PSF membranes. However, BMI is approximately not soluble in solvents such as water, EtOH, and hexanes used after membrane coagulation. Another possibility might be the presence of residual NMP in PSF membranes. The spectrum of PSF-BMI-EtOH-S membrane was observed to have a higher intensity in the range of 399–400.2 eV than spectrum of PSF-BMI-EtOH-L. This might be attributed to imide nitrogen that was partially protonated or involved in hydrogen bonding as illustrated elsewhere.<sup>63</sup> However, the increase in the intensity of the spectrum of PSF-BMI-EtOH-L at a higher range might be attributed to the presence of additional residual NMP in this membrane.

The core-level spectra of elemental sulfur were shown in Figure 8. The characteristic sulfone doublet bands were observed centered at 168.1 and 169.2 eV, which agrees well with literature.<sup>32</sup> The decrease in the intensity of these bands for membranes containing BMI might be attributed to the absence of sulfur in the BMI additive. It was clear from all above XPS results that the chemical structure on the surface of membrane agree well with the predicted theoretical composite structure. This might indicate that the surface chemical structure of membranes was not different from the structure of the corresponding bulk composites under the used XPS test conditions.

### Phase structure and thermal analysis

Surfaces of all membrane samples were examined by optical microscope. Phase separation was not observed in PSF-BMI semi-IPN membranes that were cast after 40 days. The appearance of the surface of these membranes was similar to surfaces of membranes prepared from PSF without adding BMI. Membranes containing BMI and cast after long time (100 days) for PSF had brown to orange-red dispersed

**TABLE III**  
Stoichiometric Atomic Concentration of Different Elemental Chemical States for Different Components

Component	Formula	Total atoms	Theoretical atomic concentration, %					
			Carbon atoms			Oxygen atoms		Nitrogen atoms
			CC, CH, C=C	CN, CO	OC=O, NC=O	Carbonyl	Ether or OH	Imide or amide
PSF	C <sub>27</sub> O <sub>4</sub> S	32	65.6	12.5	0	0	6.2	0
BMI	C <sub>21</sub> O <sub>4</sub> N <sub>2</sub>	27	55.5	7.4	14.8	14.8	0	7.4
NMP	C <sub>5</sub> O <sub>1</sub> N <sub>1</sub>	7	28.6	28.6	14.3	14.3	0	14.3
<i>i</i> -PrOH	C <sub>3</sub> O <sub>1</sub>	4	50.0	25.0	0	0	25	0
EtOH	C <sub>2</sub> O <sub>1</sub>	3	33.3	33.3	0	0	33.3	0



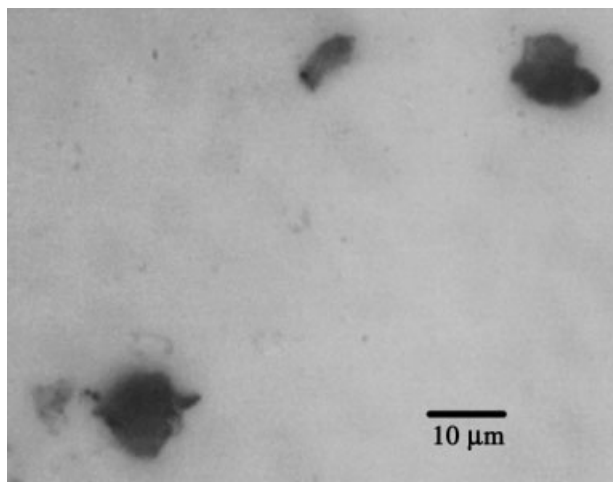


**Figure 9** Optical micrographs at 1000 times magnifications for the skinned surface of PSF-BMI-EtOH semi-IPN membrane made from a solution that showed phase separation due to prolonged mixing.

phase in some areas that represented thermoset BMI phase within a large area of continuous PSF phase. This dispersed phase had circular or cylindrical shape and some of them could be seen with size that may slightly exceed  $10\ \mu\text{m}$  as shown in Figure 9. The phenomenon of phase separation, resulted from coalescing BMI thermoset phase, influenced the membrane performance for gas separation as found through our preliminary experiments. We believe that polymeric solutions should be coagulated before the stage of significant thermoset/thermoplastic phase separation to form gas separation membranes.

Glass-transition temperature was also determined for these membranes from DSC curves as shown in Figure 10. The measured  $T_g$  of PSF-EtOH was  $185^\circ\text{C}$ , which was equal to the  $T_g$  of this polymer as reported elsewhere.<sup>18,41</sup> The  $T_g$  of PSF-BMI-EtOH-S was measured to be  $183^\circ\text{C}$ , which was lower than the  $T_g$  of PSF by only  $2^\circ\text{C}$ . This indicates a slight plasticizing effect of BMI on PSF. On the other hand, the  $T_g$  of PSF-BMI-EtOH-L was measured to be  $189^\circ\text{C}$ , which was higher than the neat PSF by  $4^\circ\text{C}$ . This might be attributed to the formation of a rigid microphase of BMI resin with a higher softening point,  $T_{g2}$  than the  $T_g$  of PSF that might restrict chain mobility of PSF. The  $T_g$  of neat BMI resin was reported to be  $399^\circ\text{C}$ .<sup>64</sup> It was clear that the  $T_g$  of base polymer could be improved through synthesis of PSF-BMI semi-IPN. The improvement might depend on the formation of rigid microphase dispersed in a base polymer such as PSF. The size of this microphase might have an important role on the properties of thermoset/thermoplastic composites. In case microphase comprised a low-molecular-weight BMI oligomer, it might act as a plasticizer that led to a decrease in the  $T_g$ ; however if the microphase was

large enough to form rigid domain, it might act as reinforcing particles that led to increase  $T_g$  compare to  $T_g$  of base polymer. The FTIR-ATR and XPS analysis revealed the presence of small residual amounts of amic acid and complexed NMP but the increase in  $T_g$  of PSF-BMI-EtOH-L indicates that these residuals were only located at BMI/PSF interface that strengthen the adhesion of two domains rather plasticizing one of the two phases. In both cases, the microphase domain size should not exceed the resolution of optical microscope to maintain interpenetrating interactions of different components within the network. Also a larger size for the thermoset phase would lead to a traditional polymer blend losing the beneficial features of semi-IPN.

### Gas transport characteristics

Gas transport characteristics including sieving properties of the novel semi-IPNs were analyzed through gas permeation tests. Gas permeance and  $\text{O}_2/\text{N}_2$  selectivity for separation of oxygen from air are shown in Table IV. It is clear that the BMI/PSF semi-IPN prepared using ethanol has the highest permeance at 553 GPU than all other structured materials. Although permeance was increased by more than 12 times over the PSF-EtOH membranes, the  $\text{O}_2/\text{N}_2$  selectivity remained same. The increase in gas permeance could be attributed to the increase in the free volume or pore number in membrane materials resulted from formation of thermoset/thermoplastic semi-IPN structure upon incorporation of BMI. Because the  $\text{O}_2/\text{N}_2$  selectivity was not decreased, presence of larger pores particularly at the interface between the two phases, was ruled out. Comparing the performance of these

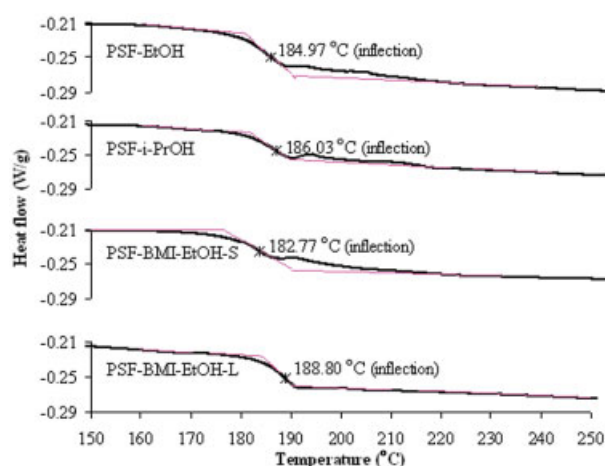


**Figure 10** DSC curves and glass-transition temperatures of PSF and their BMI semi-IPNs membranes as measured at a heating rate of  $10^\circ\text{C}/\text{min}$  in nitrogen. [Color figure can be viewed in the online issue, which is available at [www.interscience.wiley.com](http://www.interscience.wiley.com).]

TABLE IV  
Gas Permeance vs. O<sub>2</sub>/N<sub>2</sub> Selectivity for the Separation of Oxygen from Air

Membranes	Total permeance (GPU) <sup>a</sup>	Oxygen permeance (GPU) <sup>a</sup>	O <sub>2</sub> /N <sub>2</sub> selectivity
PSF-EtOH	44 ± 4	29 ± 3	1.9 ± 0.5
PSF-BMI-EtOH-S	153 ± 10	103 ± 10	2.1 ± 0.5
PSFBMI-EtOH-L	553 ± 15	366 ± 15	1.9 ± 0.5
PSF-i-PrOH	52 ± 4	34 ± 3	1.9 ± 0.5
Composite membrane <sup>63</sup>	–	33.2	4.3
	–	12	6.9
Polymeric blends membranes <sup>64</sup>	–	121	2.1
	–	127	1.5

$${}^a\text{GPU, gas permeation unit; GPU} = 1 \times 10^{-6} \frac{\text{cm}^3 (\text{STP})}{\text{cm}^2 \text{Sec cm Hg}}$$

novel membranes with reported patents, it is clear that obtaining high O<sub>2</sub>/N<sub>2</sub> selectivity of 4.3, the oxygen permeance would not exceed 34 GPU as reported elsewhere.<sup>65</sup> However as reported elsewhere,<sup>66</sup> there was a decrease in selectivity of oxygen over nitrogen to 1.5 when permeance reached 127 GPU which could be attributed to the traditional trade off known for most polymeric materials used in gas separation membranes.<sup>67</sup> The gas permeance for PSF-BMI-EtOH-L was 553 GPU that included 366 GPU of pure oxygen in the mixture with a calculated selectivity of 2.1 as shown in Table IV. Both PSF-BMI-EtOH-S and PSF-BMI-EtOH-L membrane had significantly higher permeance and selectivity than polyimide blends membranes<sup>66</sup> as seen in Table IV. The BMI/PSF semi-IPN reported in this work was tested again for air separation after 1 month and showed the same performance, indicating its good stability. Finally, these results suggest that the novel BMI/PSF semi-IPNs are a very promising polymeric material suitable for preparation of gas separation membranes.

### CONCLUSIONS

It was concluded that BMI/PSF semi-IPN membranes could be formed through *in situ* polymerization of BMI inside PSF solutions. Both PSF and a proton donor accelerate polymerization of BMI at ambient conditions without the need for an initiator or a catalyst. The polymerization of BMI was influenced by the polarity of proton donor and EtOH led to anionic polymerization mechanism. FTIR-ATR and XPS revealed that polymerization of BMI at longer stage might accompany with imide cleavage and amic acid formation while XPS results revealed that the imide nitrogen of BMI was protonated at an earlier stage as in the case of the PSF-BMI-EtOH-S membranes. It was also found that the formed amic acid has propensity to complex with NMP and EtOH. Optical microscopy showed that growth of the thermoset BMI phase within PSF thermoplastic has a significant influence

on phase separation, gas transport, and glass-transition temperature. Finally it was concluded that BMI-thermoplastic semi-IPNs are promising materials to produce high-productivity gas separation membranes.

The authors are thankful to Mr. David Kingston and Dr. Farid Benesbaa for their help with XPS/SME and FTIR-ATR experiments, respectively.

### References

- Paul, D.; Sikdar, S. K. *Clean Prod Processes* 1998, 1, 39.
- Stern, S. A. *J Membr Sci* 1994, 94, 1.
- Baker, W. R. *Ind Eng Chem Res* 2002, 41, 1393.
- Kapantaidakis, G. C.; Koops, G. H. *J Membr Sci* 2002, 204, 153.
- Pernot, H.; Baumert, M.; Court, F.; Leibler, L. *Nature Mater*, 2002, 1, 54.
- Sperling, L. H. *Interpenetrating Polymer Networks and Related Materials*; Plenum: New York, 1981.
- Sperling, L. H. In *Interpenetrating Polymer Networks*; Klempner, D., Sperling, L. H., Utracki, L. A., Eds.; American Chemical Society: Washington, DC, 1994; ACS Advances in Chemistry Series, Vol. 239, p 3.
- Lodge, T. P. *Macromol Chem Phys* 2003, 204, 265.
- Yen, C. T.; Chen, W. C.; Liaw, D. J.; Lu, H. Y. *Polymer* 2003, 44, 7079.
- Jeon, H. K.; Kim, J. K. *Macromolecules* 2000, 33, 8200.
- Lee, D. S.; Jung, D. S.; Kim, T. H.; Kim, S. C. *J Membr Sci* 1991, 60, 233.
- Lee, D. S.; Kang, W. K.; An, J. H.; Kim, S. C. *J Membr Sci* 1992, 75, 15.
- Lee, D. S.; An, J. H.; Kim, S. C. In *Interpenetrating Polymer Networks*; Klempner, D., Sperling, L. H., Utracki, L. A., Eds.; American Chemical Society: Washington, DC, 1994; ACS Advances in Chemistry Series, Vol. 239, p 463.
- Lim, B. Y.; Kim, S. C. *J Membr Sci* 2002, 209, 293.
- Mai, K.; Huang, J.; Zeng, H. *J Appl Polym Sci* 1997, 66, 1965.
- Bauer, B. J.; Briber, R. M.; Dickens, B. In *Interpenetrating Polymer Networks*; Klempner, D., Sperling, L. H., Utracki, L. A., Eds.; American Chemical Society: Washington, DC, 1994; ACS Advances in Chemistry Series, Vol. 239, p 179.
- Viot, J. F.; Seferis, J. C. *J Appl Polym Sci* 1987, 34, 1459.
- Gaina, V.; Gaina, C.; Stoleriu, A.; Timpu, D.; Sava, M.; Rusu, M. *Polym Plast Technol Eng* 1999, 38, 927.
- Liou, H. C.; Ho, P. S.; Tung, B. *J Appl Polym Sci* 1998, 70, 261.

20. Bonnet, A.; Pascault, J. P.; Sautereau, H.; Camberun, Y. *Macromolecules* 1999, 32, 8524.
21. Sommerfeld, E. G. U.S. Pat. 6,228,919 (2001).
22. Zhang, H.; Anazawa, T.; Watanabe, Y.; Miyajima, M. U.S. Pat. 6,319,404 (2001).
23. Aykurt, M.; Küçük, I.; Kuyulu, A. *Polym Bull* 2000, 44, 325.
24. Wang, D.; Li, K.; Teo, W. K. *J Membr Sci* 1995, 98, 233.
25. Tawney, P. O.; Snyder, R. H.; Conger, R. P.; Leibbrand, K. A.; Stiteler, C. H.; Williams, A. R. *J Org Chem* 1961, 26, 15.
26. Hayon, E.; Simic, M. *Radiat Res* 1972, 50, 464.
27. Ayscough, P. B.; English, T. H.; Lambert, G.; Elliot, A. J. *J Chem Soc Faraday Trans* 1977, 73, 1302.
28. Rozenberg, B. A.; Dzhavadyan, E. A.; Morgan, R.; Shin, E. *Polym Adv Technol* 2002, 13, 837.
29. Wang, X.; Chen, D.; Ma, W.; Yang, X.; Lu, L. *J Appl Polym Sci* 1999, 71, 665.
30. Melin, A. M.; Perromat, A.; Deleris, G. *Can J Physiol Pharmacol* 2001, 79, 799.
31. Maradiya, H. R.; Patel, V. S. *J Serb Chem Soc* 2002, 67, 17.
32. Song, Y. Q.; Sheng, J.; Wei, M.; Yuan, X. B. *J Appl Polym Sci* 2000, 78, 979.
33. de Kok, M. M.; van Breemen, A. J. J. M.; Carleer, R. A. A.; Adriaensens, P. J.; Gelan, J. M.; Vanderzande, D. J. *Acta Polym* 1999, 50, 28.
34. Kapantaidakis, G. C.; Kaldis, S. P.; Dabou, X. S.; Sakellaropoulos, G. P. *J Membr Sci* 1996, 110, 239.
35. Mohr, J. M.; Paul, D. R.; Pinnau, I.; Koros, W. J. *J Membr Sci* 1991, 56, 77.
36. Kim, J. H.; Kim, Y. H.; Kim, Y. J.; Won, J. C.; Choi, K. Y. *J Appl Polym Sci* 2004, 92, 178.
37. Smith, B. *Infrared Spectral Interpretation: A Systematic Approach*; CRC Press: Boca Raton, FL, 1999.
38. del Arco, M.; Carriazo, D.; Gutiérrez, S.; Martín, C.; Rives, V. *Phys Chem Chem Phys* 2004, 6, 465.
39. Wang, Z.; Chen, T.; Xu, J. *J Appl Polym Sci* 1997, 63, 1127.
40. Ha, K.; West, J. L. *J Appl Polym Sci* 2002, 86, 3072.
41. Hamerton, I.; Klewpatinond, P. *Polym Int* 2001, 50, 1309.
42. Morgan, R. J.; Shin, E. E.; Rosenberg, B.; Jurek, A. *Polymer* 1997, 38, 639.
43. Drukker, E.; Green, A. K.; Marom, G. *Compos A* 2003, 34, 125.
44. Coates, J. In *Encyclopedia of Analytical Chemistry*; Meyers, R. A., Ed.; Wiley: Chichester, 2000; p 10815.
45. Major, J. S.; Blanchard, G. *J Chem Mater* 2002, 14, 2567.
46. Akyuz, S.; Akyuz, T. *J Inclusion Phenom Mol Recognit Chem* 2004, 48, 75.
47. Corsaro, C.; Parker, S. F. *Phys B: Condens Matter* 2004, 350, e591.
48. Grenier-Loustalot, M.-F.; Gillard, M.; Joubert, F.; Grenier, P. *J Polym Sci Part A: Polym Chem* 1993, 31, 2839.
49. Ponzio, E. A.; Echevarria, R.; Morales, G. M.; Barbero, C. *Polym Int* 2001, 50, 1180.
50. Musto, P.; Karasz, F. E.; MacKnight, W. J. *Polymer* 1993, 34, 2934.
51. Shin, T. J.; Ree, M. *Macromol Chem Phys* 2002, 203, 791.
52. Johnson, C.; Wunder, S. L. *J Polym Sci Part B: Polym Phys* 1993, 31, 677.
53. Agapov, O. A.; Babaevskii, P. G.; Zhukov, A. A.; Korneeva, G. A.; Korovina, I. Y.; Chetverov, Y. S. *High Energy Chemistry* 2004, 38, 124.
54. Thomas, R. R.; Buchwalter, S. L.; Buchwalter, L. P.; Chao, T. H. *Macromolecules* 1992, 25, 4559.
55. Likhatchev, D.; Gutierrez-Wing, C.; Kardash, I.; Vera-Graziano, R. *J Appl Polym Sci* 1996, 59, 725.
56. Vora, R. H.; Goh, S. H.; Chung, T. S. *Polym Eng Sci* 2000, 40, 1318.
57. Healy, D.; Bloor, D.; Gray, D.; Cross, G. H. *J Phys D: Appl Phys* 1997, 30, 3079.
58. Bu, X. H.; Du, M.; Zhang, L.; Liao, D. Z.; Tang, J. K.; Zhang, R. H.; Shionoya, M. *J Chem Soc Dalton Trans* 2001, 5, 593.
59. Burrell, M. C.; Chera, J. J. *Surf Interface Anal* 1999, 27, 811.
60. Bubert, H.; Lambert, J.; Burba, P.; Fresenius, J. *Anal Chem* 2000, 368, 274.
61. Vinnichenko, M.; Chevolleau, T.; Pham, M. T.; Poperenko, L.; Maitz, M. F. *Appl Surf Sci* 2002, 201, 41.
62. Xiao, S. J.; Textor, M.; Spencer, N. D.; Wieland, M.; Keller, B.; Sigrist, H. *J Mater Sci: Mater Med* 1997, 8, 867.
63. Wang, W. C.; Vora, R. K. H.; Kang, E. T.; Neoh, K. G. *Macromol Mater Eng* 2003, 288, 152.
64. Pascal, T.; Mercier, R.; Sillion, B. *Polymer* 1990, 31, 78.
65. Ding, Y.; Bikson, B.; Nelson, J. K. U.S. Pat. 6,790,263 (2004).
66. Ekiner, O. *Eur. Pat. Appl.* 0,648,812 A3 (1994).
67. Robeson, L. M. *J Membr Sci* 1991, 62, 165.